Journal of CO2 Utilization 82 (2024) 102770

Contents lists available at ScienceDirect

Journal of CO2 Utilization

journal homepage: www.elsevier.com/locate/jcou

A thorough assessment of mineral carbonation of steel slag and refractory waste

Santiago Capelo-Avilés [a,b,c], Raiana Tomazini de Oliveira [a], Irene I. Gallo Stampino [a], Francesc Gispert-Guirado [d], Anna Casals-Terré [b], Stefano Giancola [e,*], José Ramón Galán-Mascarós [a,f,**]

[a] Institute of Chemical Research of Catalonia (ICIQ-CERCA), Avinguda Països Catalans 16, Tarragona 43007, Spain
[b] Compañia Española de Laminación S.L (CELSA), Spain
[c] Departament de Química Física i Inorgànica, Universitat Rovira i Virgili, Marcel. lí Domingo 1, Tarragona 43007, Spain
[d] SRCIT-URV, Avinguda Països Catalans 26, Tarragona 43007, Spain
[e] Orchestra Scientific SL, Avinguda Països Catalans 16, Tarragona 43007, Spain
[f] Catalan Institution for Research and Advanced Studies (ICREA), Passeig Lluís Companys 16, Barcelona 08007, Spain

ARTICLE INFO

Keywords:
CO_2 capture and utilization
Steel slags carbonation
Circular economy
CO_2 mineralization
Industrial wastes valorisation

ABSTRACT

Escalating industrial CO_2 emissions necessitate innovative carbon capture and utilization strategies. This study explores the potential of mineral-carbonation of steelmaking slags, particularly White Slag (WS) and various Refractory Wastes (RWs), to mitigate CO_2 emissions and valorize industrial wastes. Experiments were performed with waste materials from the production lines at CELSA (Barcelona, Spain). We delved into direct aqueous carbonation, evaluating the performance and characteristics of these wastes under different experimental conditions. Our findings reveal that all slags can effectively sequester CO_2. This process is effective not only for pure CO_2 but also for diluted flue gases under mild conditions ($\leq$ 100 ºC, $\leq$ 6 bar). Specifically, WS exhibited peak CO_2 sequestration capacities (SC) of 359.79 gCO_2/kgslag (pure CO_2) and 276.65 gCO_2/kgslag (diluted flue gas). In contrast, the RWs presented different kinetic, reaching a maximum SC of 311 gCO_2/kgslag after prolonged times. Given the large inhomogeneity of RWs, individual analysis of distinct RW fractions revealed significant variations in carbonation performance. Tundish RW exhibited the highest CO_2 sequestration capacity, emphasizing the importance of waste source and mineral composition in the carbonation. Chemical and morphological evaluations confirmed the transformation of CaO to $CaCO_3$, with MgO remaining largely inert. Additionally, the process indicated potential environmental benefits by reducing the mobility of toxic metals, particularly Pb, suggesting an ancillary avenue for waste treatment. This study underscores the utility of CO_2 mineralization as a dual-benefit approach within the circular economy framework, offering insights into its application for sustainable waste management and CO_2 emission reduction in the steel industry.

1. Introduction

Global emissions from fossil fuel combustion and industrial activities surpass 36.5 $GtCO_2$ annually [1]. In this context, adopting a circular carbon economy is vital for enhancing industrial sustainability. The concept emphasizes transforming waste into green valuable resources, crucial for reducing carbon footprints [2]. Specifically, CO_2 mineralization offers a pragmatic approach to advance the circular economy by carbon capture, storage, and utilization, while simultaneously establishing a waste-to-resource supply chain [3]. In this line, the utilization of industrial solid wastes as capture media is particularly appealing [4,5]. Multiple industrial wastes may react with CO_2 to yield a variety of carbonates [6], adding value to the steel [7], metallurgy [8], cement [9,10] and mining industries [11], to name a few. Promising perspectives are open for alkaline solid wastes in CO_2 mineralization, as a process able to reduce atmospheric CO_2 while transforming the industrial wastes into valuable construction materials [12–14]. Life cycle analysis (LCAs) indicate that these processes would be sustainable

* Corresponding author.
** Corresponding author at: Institute of Chemical Research of Catalonia (ICIQ-CERCA), Avinguda Països Catalans 16, Tarragona 43007, Spain.
E-mail addresses: sgiancola@orchestrasci.com (S. Giancola), jrgalan@iciq.es (J.R. Galán-Mascarós).

https://doi.org/10.1016/j.jcou.2024.102770
Received 8 January 2024; Received in revised form 11 April 2024; Accepted 15 April 2024
Available online 17 April 2024

[15–18], working towards a circular, climate-optimal economy [19,20] with a Net-emission reduction [21]. Globally, such a technology could reduce 4.02 $GtCO_2$ per year, corresponding to the 12.5% of the anthropogenic global CO_2 emissions [22]. Even CO_2 direct air capture has been proven as feasible [23].

The steel industry, responsible for nearly 2.9 $GtCO_2$ or 8 % of worldwide emissions [24,25], is progressing in emission reduction through improved process efficiencies. Nonetheless, these efforts are inadequate against set decarbonization objectives [1,24,26–28]. Moreover, based on recent estimations [22], 43.5 % of the amount of direct CO_2 reduction could be just ascribed to the mineralization of iron and steel slags. Therefore, the integration of carbon capture and storage management protocols into the circular economy framework is crucial for aligning with and accomplishing environmental goals [22,29]. About 32.4 % of total Steel production consists of by-products (slag, dust, process gas, etc.), with another 2.7 % classified as currently non-recoverable waste [30,31]. Initially, steel slag was considered waste and used to be disposed of in landfills [25]. However, modern efforts are redirecting some types of slag away from landfills and instead using them as green cementitious materials and quarry fillers [25,32,33]. In addition to their uses in building materials, there are a variety of interesting potential applications for steel slag, not limited to CO_2 mineralization [34–36], but also covering nutrient recovery [37], wastewater treatment [38], and soil enhancement [39]. Consequently, effectively utilizing and managing slag has become a pivotal concern within the steelmaking industry. Several studies prove that treating steel slag through carbonation improves its properties, including enhanced hardness and chemical reactivity [40,41]. This development is promising for future applications, such as pavement, cement, and the manufacturing of concrete products [32,42,43].

Slag–carbonation studies have received considerable attention in the waste management and environmental sustainability fields due to the remarkable opportunities it is offering. However, some barriers still need to be overcome for this technology to be effectively applied on an industrial scale. In particular, it's large scale adoption, requires a careful evaluation of the carbonation potential of the different residues of several industries as well as the determination of the optimal operating conditions to reduce the energy requirement [22,44]. Indeed, although numerous studies [41,42,45–52] have comprehensively analyzed the carbonation processes of slags, there is still a notable gap in the literature regarding the detailed analysis of these wastes, their origins, and their intrinsic properties. Furthermore, research specifically targeting the slag generated in the secondary steel industry using low-concentration flue gas (<15 % CO_2) is scarce. Most mineralization studies have focused on slag from the primary steel industry, which involves off-gas streams with high carbon dioxide concentrations. In addition, no special attention has been paid to refractory waste as a potential candidate for CO_2 mineralization. Traditionally, Electric Arc Furnace (EAF) and Basic Oxygen Furnace (BOF) route slags have often been discussed together, and their properties are attributed to the total slag output of a particular steelmaking process [53,54]. However, it is essential to recognize that each slag is derived from a separate sub-process stream. As we will explore in this article, the source of the slag has a significant impact on its unique properties, which influence its potential for valorization in several ways. White slag (the slag from the ladle furnace) is the material most often subjected to mineralization reaction analysis. Still, refractory waste (the residue adhering to the refractories of the furnace) holds promise as a suitable candidate for mineralization, as does white slag, which has elevated basicity owing to the presence of metal oxides (e.g., CaO, MgO).

This gap in understanding the provenance and independent valuation of steel slags, from both a practical industrial and academic perspective, requires more focused studies. The fusion of these two perspectives is crucial for achieving a holistic understanding of waste valorization and to boost, especially in the case of materials characterized by unique properties that make their valuation challenging. This study focuses on four different waste streams from the secondary steel industry, mainly derived from scrap and recycling processes within steel production (Fig. 1a). Among these wastes, white slag (WS) has the lowest management costs, and some of it (non-carbonated) finds application in cement plants and quarry backfills. However, a significant proportion still end up in landfills. The other three wastes came from demolishing various refractories associated with the EAF, ladle furnace, and pouring tundish. Each of these refractory waste (RW) streams has different characteristics and chemical composition profiles because of the unique interaction between the cast steel of varying chemical composition and the specific surface area of the refractories in the furnace. As a result, the cost of managing these RW materials varies, with tundish RW having the highest price and management complexity, primarily due to its high lead (Pb) content. To optimize waste management costs and reduce the concentration of leached heavy metals (e.g., Cr, Pb), secondary steel companies often mix this three RW material streams into a single waste category called "refractory waste". This pragmatic approach helps to dilute the heavy metal concentrations, which is particularly important given that almost all of this waste ends up in landfills. Fig. 1b shows the CO_2 equivalent emission factor associated with the primary raw materials used in steel production. In particular, the use of methane as a fuel source, mainly in the reheating furnaces of the rolling mills, turns out to be the largest contributor to CO_2 emissions within the secondary steel industry. Fig. 1c provides an overview of the annual management costs of the main wastes in real steel industry. Among these wastes, white slag and refractory waste have the highest annual management costs of 307k€ and 486 k€, respectively. This contextual information underlines the potential of CO_2 mineralization as a promising strategy for simultaneously addressing waste management challenges and reducing CO_2 emissions in a real industrial environment.

The composition of slag varies depending on the specific process, but it generally contains large amounts of calcium (Ca) and magnesium (Mg) in various forms, such as oxides, hydroxides, silicates, and aluminosilicates [35,40,55,56], as well as remnants from the steel production process (Fe, Mn, Cr, Ti, S, V, Mn, among others). There are two main methods of slag carbonation in the steel industry: direct and indirect. The indirect route involves the extraction of Ca^+ and Mg^+ ions under acidic conditions, followed by a reaction with CO_2 to form highly pure carbonates [25,40,54,57–60]. This method typically incurs higher costs [25,35]. In contrast, the direct method includes mineralization reactions within the slag, eliminating the need for metal removal. This route is divided into two distinct variants: solid-gas contact (with moisture content less than 0.2) and solid-liquid-gas interaction, known as aqueous mineral carbonation. Compared to the indirect route, which relies on a continuous supply of acids for metal extraction, this route offers a clear competitive advantage when performed at the source of the waste. However, the resulting carbonates often lack the high purity required for specific applications, such as food and pharmaceutical industries [53]. Nevertheless, they find valuable utility in other applications, such as construction and soil additive compounds [40,41,53]. We focused primarily on direct carbonation due to its advantages, including cost-effectiveness and achieving high carbonation degrees in a shorter timeframe. Specifically, we employ direct aqueous carbonation, as the presence of water promotes ion dissolution, facilitating the formation of carbonate ions, resulting in faster carbonation rates and higher carbonation degrees [40,45,46,56,61].

In the aqueous phase, the main mineralization reaction, as described in Eq.1, involve the initial hydration of free calcium and magnesium oxides (f-CaO/MgO) to form $Ca(OH)_2$ and $Mg(OH)_2$, respectively, followed by carbonation to $CaCO_3$ and $MgCO_3$ [25,41]. However, although $MgCO_3$ has a lower enthalpy of formation (–118 kJ/mol) compared to $CaCO_3$ (–179 kJ/mol), the charge density of Mg^{2+} presents challenges to the reaction kinetics due to the smaller ionic size and higher lattice, and hence the resulting enthalpy. The conversion of MgO to $MgCO_3$ requires a change in the MgO lattice, a process that does not readily occur under

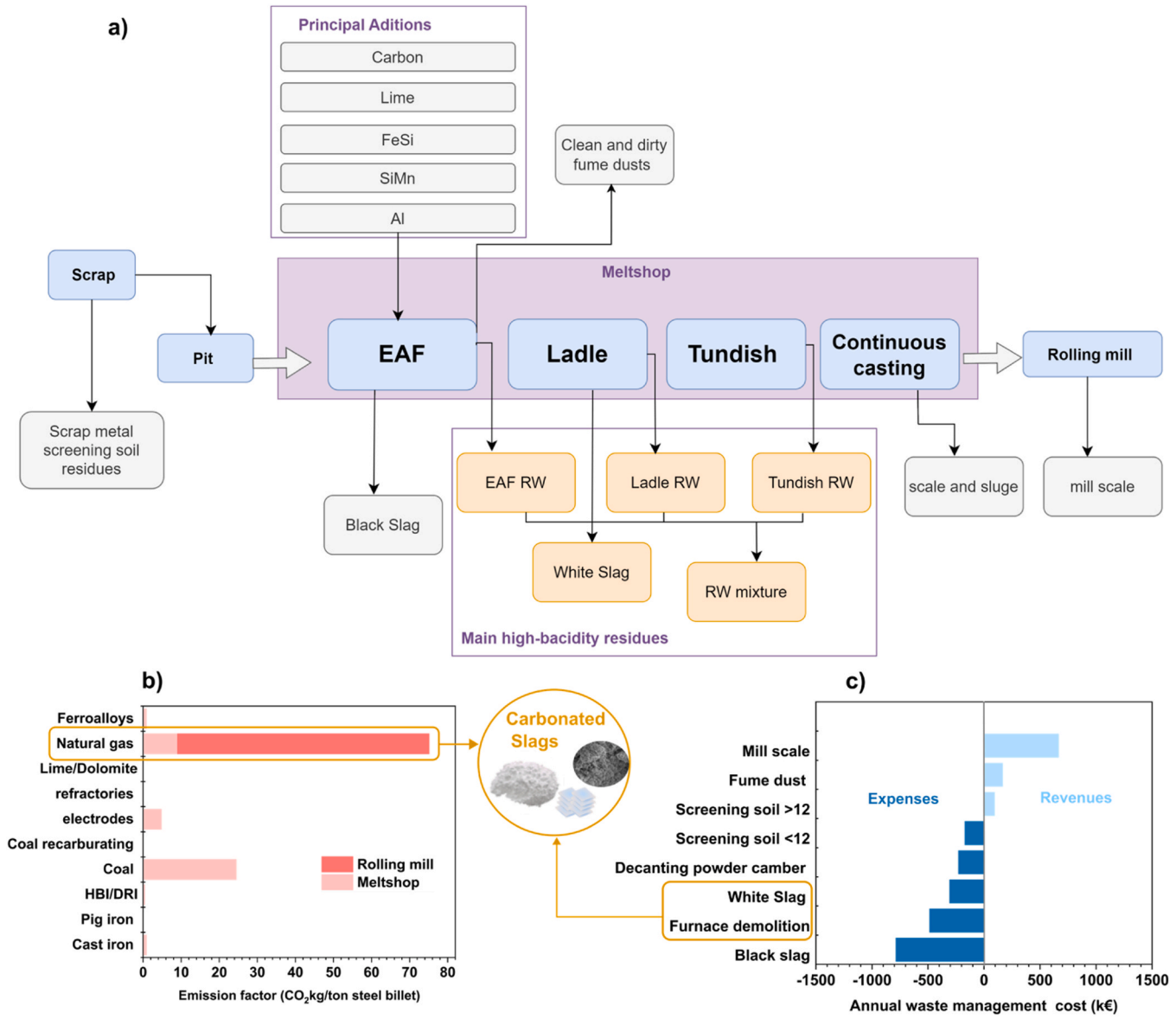

Fig. 1. a) Flow diagram of steel industry waste origins, b) CO_2 equivalent emission factor for raw materials in billet production, and c) Annual waste management cost in the steel industry (Negative values indicate losses, positives values indicate income from waste management). Data for this figure was provided by CELSA with their permission.

standard conditions. Surprisingly, MgO remains almost unchanged even when exposed to 1 atm CO_2 over a temperature range from room temperature to 500 °C. Attempts to improve the reaction rate by increasing the surface area of MgO have had limited success. Although increasing the pressure could accelerate the reaction, it may not be viable for practical applications [62,63]. Consequently, under mild conditions, mineralization is almost always associated with converting CaO to $CaCO_3$, as will be discussed in this article. Several important intermediate products have arisen during these reactions, as documented in previous research [25,40,64]. Furthermore, it is crucial to underline the importance of material composition and crystalline structure, which profoundly influence the mineralization of CO_2 steel industry slag [25].

$$(Ca,Mg)_xSi_yO_{x+2y+z}H_{2z(s)} + xCO_{2(g)} \rightarrow x(Ca,Mg)CO_{3(s)} + ySiO_{2(s)} + zH_2O_{(l)} \quad (1)$$

In this context, the present study aims to boost the implementation of CO_2 mineralization of basic wastes by providing valuable insights into the sustainable management of secondary steel industry waste and reducing CO_2 emissions, ultimately promoting environmentally responsible and economically viable waste valorization. In particular, we investigate the CO_2 sequestration capabilities of four steelmaking by-products: white slag, Tundish RW, ladle RW, and EAF RW. We conduct a detailed analysis of how different process parameters influence mineralization. We employ diverse analytical methods to assess the composition and structure of both carbonate and non-carbonate phases in the slags and associated residual water. Our research prioritizes mild operational conditions to underscore the techno-economic viability of these materials' valorization through CO_2 mineralization. Uniquely, we evaluate each waste's reactivity, individually and in combination (specifically for RW), acknowledging their distinct origins and properties. Contrasting with the broad generalizations in existing literature, our analysis elucidates the distinct CO_2 sequestration potentials inherent to each specific waste type, thereby advancing more targeted and effective strategies for their utilization.

2. Materials and methods

2.1. Materials

The solid by-products White Slag (WS) and refractories wastes (RWs) were procured from Compañia Española de Laminación S.L (CELSA), located in Barcelona, Spain. The RW encompasses three distinct types of refractories sourced from various stages in the steel production process: Tundish furnace refractories waste (TRW), Electric arc furnace refractories waste (ERW), and Ladle furnace refractories waste (LRW). For clarity in subsequent references, the abbreviation RWs signifies the composite of these three refractories wastes. To ensure sample homogenization, both WS and RWs samples underwent ball mill grinding at a rate of 15 s^{-1} during 30 min, followed by sieving with a 200 μm mesh size. Post-screening particle size distribution analysis shows that the average particle size for non-carbonated WS and RW is 167 μm and 35–37 μm, respectively. The processed samples were then securely stored within capped containers, ensuring their consistency throughout the course of the study.

2.2. Experimental procedure

2.2.1. Slurry formation

Deionized water was employed to create the WS and RW slurries. Each sample (WS and RWs) was thoroughly mixed with deionized water at a designated liquid-to-solid (L/S) ratio. The pH of the suspension was measured before introducing it into the mineralization reactor. The experiments were carried out using ratios of 5, 10, 20, 30, and 35 ml/g.

2.2.2. Mineralization reactor

We conducted CO_2 mineralization in a cylindrical semi-batch reactor with an inner diameter of 60 mm and length of 40 mm. A bed-type stirrer attached to a magnet at the base of the shaft equipped this reactor. A closed section in the agitator accommodates the sludge sample for carbonation. The gas is introduced through the agitator shaft and distributed inside the chamber containing the solid material, which favors the interaction between the gas, solid, and liquid phases. At the top of the reactor are three connections: two for gas inlet and outlet, and a third for pressure control. For a visual representation of the precise geometrical attributes of the reactor, see Figure S16.

2.2.3. Mineralization experiment

We conducted mineralization measurements using the experimental setup depicted in Fig. 2. We used gas cylinders containing N_2 (Praxair, 99.999 %) and CO_2 (Air Liquide, 99.998 %). A set of calibrated mass flow Precise control over the composition and flow of the inlet gas stream was achieved using a set of calibrated mass flow controllers (Bronkhorst EL-FLOW) located upstream of the separation module achieved precise control of the composition and flow rate of the inlet gas stream. We monitored the actual pressure by using the pressure gauge upstream of the reactor and managed pressure adjustments through a needle valve in the outlet gas line. All pressure values are given in absolute bar unless otherwise stated. A linear power silicone heating cable (Ø 3 mm FOR-FLEX NORMAL, Electricfor) was wrapped around the reactor to ensure efficient heating of the mineralization reactor. Temperature measurement was facilitated by a K-type thermocouple (Thermocoax) in contact with the outer wall of the reactor, under the control of an EZ-Zone temperature controller (Watlow). We initiated the reaction mixture using a magnetic stirring plate below the mineralization reactor.

For the white slag (WS), the experimental assessment encompassed two gas compositions: pure CO_2 and a CO_2 (10 %)/N_2 (90 %) mixture, designed to replicate the off-gas stream from the CELSA rolling mill furnace. We maintained a consistent total inlet gas flow rate of 100 NmL/min throughout the experiments. Initially, we conducted the experiments by varying pressures (2, 4, and 6 bar), T (25ºC, 50ºC, and

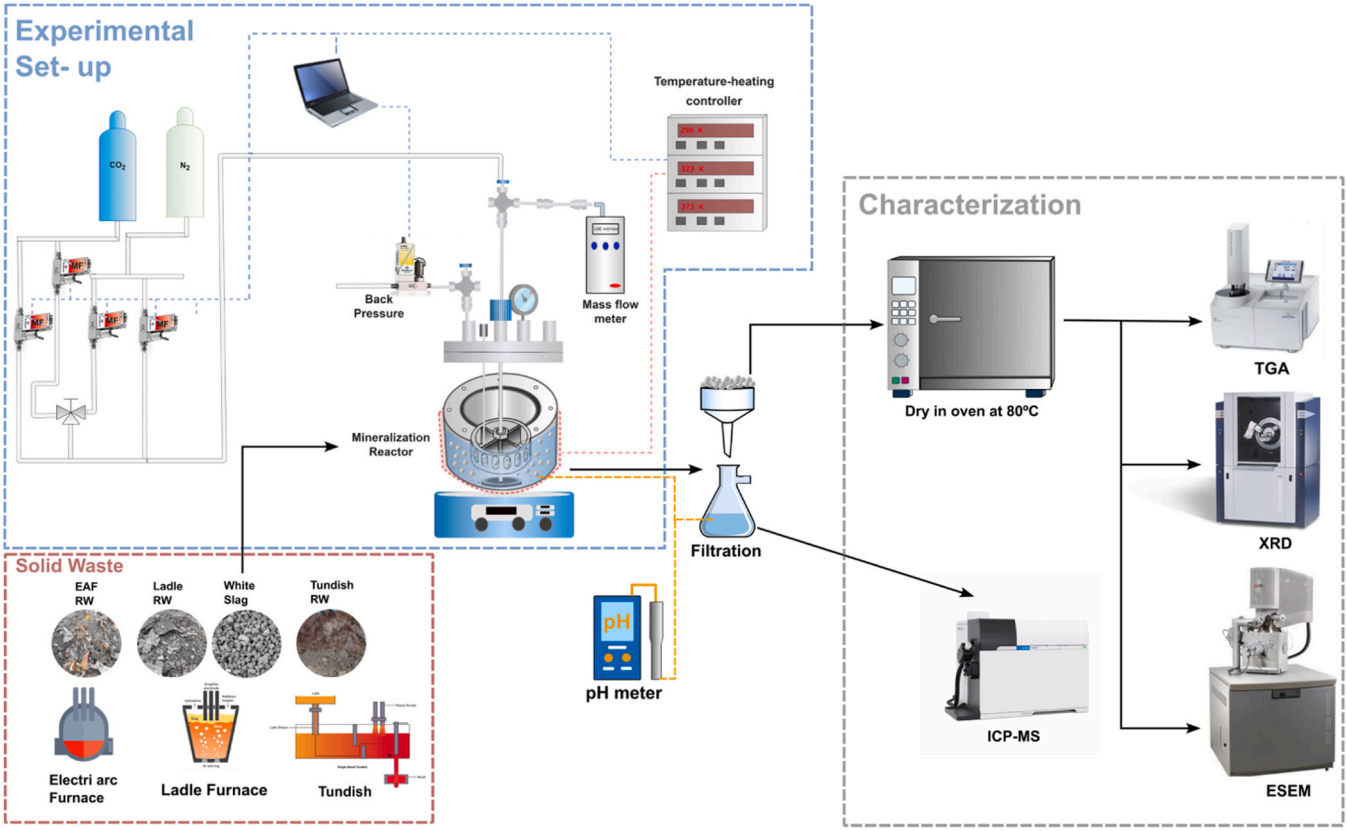

Fig. 2. Experimental Set-up for CO_2 mineralization with steel wastes and samples characterization techniques.

100ºC), stirring rate (100–600 rpm), and liquid-to-solid ratio (5–35 ml/g). Additionally, we determined the maximum carbonation capacity of the WS material through an extended 12 h experiment using pure CO_2 at 25ºC, 3 bar pressure, and 500 rpm stirring rate. After completing the initial measurement set, we also identified optimal operating conditions.

Considering the company's waste blending practice to meet environmental standards, we later investigated mineral carbonation for the refractory waste mixture (RWs) by mixing the individual refractory waste (RW) in equal proportions (33 wt% each). The RWs mixture underwent testing at different reaction times (15–390 min) and total gas pressure (2–6 bar). Furthermore, the carbonatation reaction performance of each RW was compared (conditions: 60 min and 4 bar). All experiments utilized a 20 L/S ratio and 500 rpm.

From the mineralization reaction, the reacted slurry samples of WS and RWs were promptly withdrawn and subjected to filtration through quantitative filter paper (Filter-Lab, 0.16 mm thickness, 2–4 μm pore size, 55 mm diameter). The resulting filtered carbonated material was then dried at 105ºC in an oven for 8 h and stored in a sealed container. To homogenize the dry carbonated samples for RWs, we incorporated an additional ball milling (15 s^{-1} for 30 min). Contrarily, this step remained superfluous in the case of WS samples due to their inherent homogeneity. To ensure the reliability of our results, we conducted each measurement three times. Considering these replicates, we calculated the experimental error based on the standard deviation of the measurements, which is represented by error bars in Figs. 3 and 4.

2.3. Physicochemical characterization

The thermal characteristics of both white slag and refractory wastes were analyzed before and after the carbonation process using a thermogravimetric analyzer (TGA/SDTA 851 Mettler). For each analysis, approximately 20 ± 3 mg of powdered waste was placed within alumina capsules (100 μL capacity). The analysis involved a controlled heating program, with a ramp rate of 10 °C per minute, spanning from 30 °C to 1000 °C, all conducted under a N_2 flow environment. To perform the semi-quantitative mineral composition tests, X-ray diffraction measurements (XRD) were made using a Bruker-AXS D8-Advance diffractometer with vertical theta-theta goniometer, incident- and diffracted-beam Soller slits of 2.5º, a fixed 0.5º receiving slit and an automatic Air scattering knife on the sample surface. The angular 2θ range was between 5 and 80º. The data was collected with an angular step of 0.02º at a step/time of 0.5 s. Cukα radiation was obtained from a copper X-ray tube operated at 40 kV and 40 mA. Diffracted X-rays were detected with a LynxEye-XE-T PSD detector with an opening angle of 2.94º. Quantitative phase analysis was derived from XRD powder patterns using the Rietveld refinement[65], with TOPAS v6 software. The background was modelized with a 2nd order Chebyshev polynomial. The instrumental contribution to the diffraction profile was calculated with the Fundamental Parameters Approach[66]. The relative quantitative phase analysis was obtained by refining the Rietveld scale factor for each phase and applying the corresponding well-known equations[67]. The peak width of each phase was contribution of the crystallite size effect and discarding any contribution of the microstrain to the peak width. The averaged integral breadth was obtained from the resulting fitted Voigt function to the whole diffractogram. The Scherrer equation[68] was then applied to obtain the apparent crystallite size (refer to Section 3 of the supplementary information for detailed of the Rietveld method employed). X-ray fluorescence (XRF) analysis of the four types of waste was provided by CELSA. Fourier Transform Infrared Spectroscopy (FT-IR) measurements were performed on a Bruker Optics FT-IR Alpha spectrometer equipped with a DTGS detector, KBr beam splitter at 4 cm^{-1} resolution and with a one bounce ATR accessory with diamond windows. All infrared spectra were collected in a range of wavenumber 4000 – 400 cm^{-1}. Semi-quantitative elemental analysis and morphological characterization of the sample were performed using a Field Emission Scanning Electron Microscopy-Focused Ion Beam (FESEM-FIB)

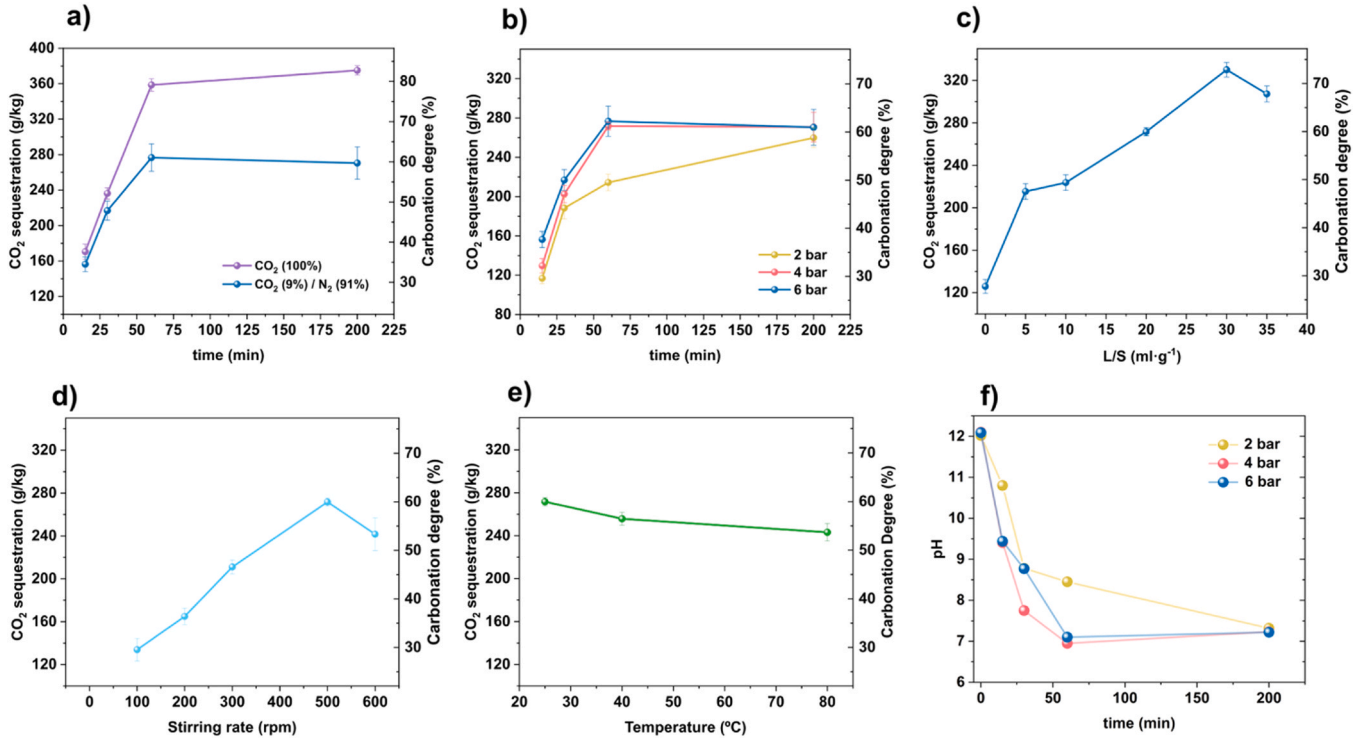

Fig. 3. a) δCaO and SC of WS using pure CO_2 and a simulated flue gas mixture; b-e) δCaO and CDSC in function of different reaction parameters using a 9 %CO_2 in N_2 gas mixture: b) At different reaction time (15–200 min) and pressure (2–6 bar), c) At different L/S ratios (with t=60 min, stirring rate=500 rpm and T=25ºC), d) At different stirring rates (with t=60 min, L/S = 20 ml/g, P = 4 bar and T = 25ºC), and e) At different temperatures (with t= 60 min, L/S = 20 ml/g, P=4 bar and Stirring rate=500 rpm); and f) pH value at different reaction times and pressures using gas mixture.

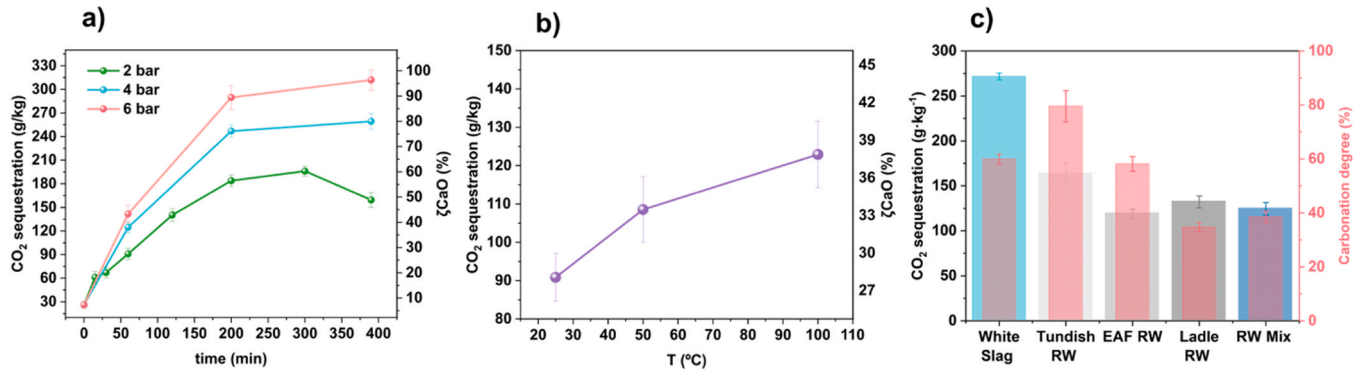

Fig. 4. Sequestration capacity (SC) and δCaO: a) RWs at different reaction times (15–390 min) and pressures (2–6 bar), b) RWmix at different temperatures (25ºC-100ºC) at 2 bar and 60 min reaction time, and c) White slag, Tundish RW, EAF RW, Ladle RW, and RWs at the same experimental conditions (4 bar, t = 60 min, and 25ºC). All experiments were performed with an L/S ratio of 20 and a stirring rate of 500 rpm.

with Scios2 FEI equipment, coupled with an electron beam and a focused Gallium ion beam. Crystal size was determined using ImageJ software. We analyzed the content of the metals in the non-carbonated samples and also the leached metals in the residual water after the mineralization reaction using Inductively Coupled Plasma Mass Spectrometry (ICP-MS) with an Agilent 7900 instrument equipped with a Micromist concentric nebulizer, Scott spray chamber, platinum interface cones, off-axis double lens system, hyperbolic quadrupole mass filter, and octopolar collision/reaction cell. A 5–10 mg sample was weighed and digested in an acidic solution using a microwave oven at 220 °C. The solution was then diluted to 5 ml with ultrapure water and analyzed. Quantification was achieved using a calibration curve spanning 0–2000 ppb. Particle size distribution (PSD) analyses were performed in a Malvern Mastersizer 2000 equipped with a Hydro 2000SM sample dispersion unit. We use approximately 100 – 200 mg of the sample with 5 ml of ethanol to prepare the emulsion.

2.4. CO_2 sequestration and carbonation degree

The CO_2 sequestration capacity (SC), quantified as the mass of CO_2 sequestered per kilogram of solid waste, was calculated using Eq.2. The CO_2(wt%) term represent the weight loss attributed to the volatilization of calcium carbonate polymorphs (Δm_{CaCO_3}) at temperature range between 500 and 900 °C [69,70], based on the dry weight at 105ºC ($m_{105°C}$) and determined by TGA (Eq.3). It is pertinent to note that the slags contain an initial $CaCO_3$ content (prior to the carbonation reaction) that varies depending on the type of slag. This value was not subtracted from the overall quantity of calcium carbonate. Moreover, the conversion of MgO to $MgCO_3$ in the waste is expected to be minimal, or absent [71]. The challenging magnesium aqueous carbonation conditions, requiring CO_2 pressures greater than 100 bar, temperature above 144ºC, and hours of reaction time, limit such conversion[40]. Therefore, the degree of carbonation (δCaO) mainly relies on the transformation of total CaO present in the sample (assuming the calcium-bearing compositions are the main reaction species). This can be calculated using Eq.4, where M_wCO_2 and M_wCaO are the molar masses of carbon dioxide and calcium oxide, respectively. CaO_{total} represents the weight fraction of calcium oxide in the solid waste sample before the carbonation reaction, expressed as percentage of dry mass and determined by XRF.

$$CO_2 sequestration \left(\frac{g_{CO_2}}{kg_{Slag}}\right) = \frac{CO_2(wt\%)}{100 - CO_2(wt\%)} \times 1000 \quad (2)$$

$$CO_2(wt\%) = \frac{\Delta m_{CaCO_3}}{m_{105°C}} \times 100 \quad (3)$$

$$\delta_{CaO} = \frac{\frac{CO_2(wt\%)}{100-CO_2(wt\%)} \times \frac{1}{Mw_{CO_2}}}{\frac{CaO_{total}}{Mw_{CaO}}} \times 100 \quad (4)$$

3. Results and discussion

3.1. Characterization of non-carbonated waste

Characterization of the different wastes before the carbonation reaction was first assessed. Particularly significant is their CaO content, since this will dominate the extent of carbonation. *White slag, (WS):* XRF analysis of white slag (table S5) reveals a total CaO amount of 58 % with trace elements (e.g., SiO_2, FeO) not expected to contribute to CO_2 sequestration[64]. The X-ray diffraction (XRD) pattern in figure S2a allowed us to precisely determine the crystalline mineral compositions with a Rietveld approach (table S4**)**. Among the primary phases that can potentially release Ca and Mg ions into the water, prominent ones include γ-Ca_2SiO_4 (27.6 %), Ca_3Mg $[SiO_4]_2$ (8.1 %), β-Ca_2SiO_4 (6.7 %), $MgSiO_3$ (5.5 %), Ca_2Al $(AlSi)O_7$ (4.1 %), among other minor components. Both γ-Ca_2SiO_4 and β-Ca_2SiO_4 are the significant phases present in OPC (Ordinary Portland Cement). Thus, Ca_2SiO_4 emerges as the predominant primary phase. These silicate species exhibit varying reactivity levels[42], influencing the overall alkalinity of the water and subsequently enhancing CO_2 retention capabilities. The sequestration capacity (SC) estimated by TGA (figure S1a) is 86.73 g_{CO2}/kg_{slag}. This corresponds to a $CaCO_3$ content of 17.5 % and a carbonation degree (δCaO) of 19.14 %. This calcium carbonate is present in the sample before the aqueous mineralization reaction in our reactor, likely resulting from a reaction that occurs when the hot and wet slag is initially generated as waste with the presence of ambient CO_2. Moreover, the ICP-MS analysis (refer to table S7) not only discloses that calcium (Ca) exhibits the highest concentration at 59.9 mg/g, but also identifies the presence of other potentially toxic metals, specifically chromium (Cr) with 189 mg/kg, nickel (Ni) with 130 mg/kg, and lead (Pb) at lower concentration 23 mg/kg.

Refractory wastes (RWs): The XRF analysis of the RWs (table S6) reveals the predominant presence of CaO, constituting 41.2 % of the total metal oxides. Additionally, a notable concentration of MgO (22.2 %) is observed, along with other metal oxides, such as Fe_2O_3 or SiO_2, that should not actively contribute to the mineralization reaction. The XRD analysis (figure S4) and its Rietveld quantification (table S2) indicate that the crystalline phases that promote Ca^+ dissociation are the γ-Ca_2SiO_4 (18.8 %) and β-Ca_2SiO_4 (8.9 %) forms, alongside minor constituents such as Portlandite, selenite, and $CaOH_2$ (6.1 %), $Ca_2Al_2SiO_7$ (2.1 %), $Ca_{12}Al_{14}O_{33}$ (6.2 %), Ca_2AlFeO_5 (3.8 %), and among others. Moreover, the principal mineral phase in the non-carbonated RWs is the MgO with 28 %. The calculated initial sequestration capacity (SC) of the

RWs is 26 g_{CO2}/kg_{slag}. This value is lower if compared to the WS. This suggests that the RWs (non-carbonated) has comparatively less reaction activity with the environment, resulting in a lower initial concentration of $CaCO_3$ (6 %) and with a degree of carbonation (δCaO) of 8 %. Further XRF analysis of individual RWs indicate that the Ladle RW with a 48.6 % CaO has the highest content of this reactive metal oxide, concerning the tundish RW (26 %) and EAF RW (23%). The mineralogical characteristics of the individual RWs (figure S2b-**d**) vary significantly, with each RW demonstrating specific traits. Comparing the RWs, the Ladle RW exhibits the lowest sequestration capacity (SC) of 22.6 g_{CO2}/kg_{slag}, accompanied by a minimal δCaO of 5.9 %. This suggests that although it contains a high concentration of CaO, a significant portion has remained unreactive with the environment. In contrast, the Tundish RW shows the highest SC value of 84 g_{CO2}/kg_{slag}, correlating with a δCaO of nearly 41 % (high environmental reaction activity). Lastly, the EAF RW displays a moderate SC of 26 g_{CO2}/kg_{slag}, with a δCaO of 14.5 %.

Upon comparing the concentration of heavy metals analyzed by ICP-MS (table S7), we note that the Cr content shows slight variations across the refractory wastes. The Tundish RW exhibits the highest value at 1.97 mg/g, followed by the EAF RW (1.71 mg/g) and the Ladle RW (0.473 mg/g). These values are notably higher than the white slag (0.18 mg/g). On the other hand, regarding Pb content, the Tundish RW has the highest concentration at 371 mg/kg. In contrast, the EAF and Ladle RWs showcase considerably lower values of 68 and 51.5 mg/kg mg/kg, respectively. This tendency often prompts industries to mix these refractory wastes, aiming to lower the heavy metal concentration to prevent their excessive leaching into the soil and subsequently curtail waste management costs, as mentioned earlier. Upon analyzing the RWs mixture, it becomes apparent that both the Cr content (1 mg/g) and Pb content (240 mg/g) are reduced from the values observed in the Tundish RW, the main source that incurs the highest management costs. Cr, Pb concentration in RWs is remarkably higher than that of WS. The morphological analysis of both the non-carbonate WS and RWs samples will be discussed in Section 3.3, contrasting their characteristics with those of their carbonated counterparts.

3.2. Carbon sequestration and carbonation degree

The carbonation reaction of WS was thoroughly investigated by examining the influence of key process parameters. Initially, we compared the mineralization performance using two different inlet gases: pure CO_2 and a gas mixture simulating typical CELSA flue gas (composed of N_2 at 90 % and CO_2 at 10 %) (Fig. 3a). Under the specified conditions (6 bar, 25 ºC, L/S = 20, 500 rpm), the reaction reached its completion (carbonation degree plateau) after 60 min with both inlet gases. When pure CO_2 was employed, the white slag achieved a maximum degree of carbonation (δCaO) of 79 %, corresponding to a CO_2 sequestration capacity (SC) of 360 g_{CO2}/kg_{slag}. In contrast, using the gas mixture resulted in a 23 % reduction in carbonation capacity (δCaO = 61 % and SC = 277 g_{CO2}/kg_{slag}), despite the significantly lower inlet CO_2 partial pressure. Notably, the difference in carbonation capacity between the two inlet gases increased as the reaction time extended (28 % after 200 min compared to 8.3 % after 15 min), indicating a faster reaction rate with pure CO_2. This discovery underscores the potential of WS for capturing CO_2 directly from flue gas, eliminating the need for a carbon dioxide pre-concentration step.

Fig. 3(b-f) illustrates the impact of pressure, temperature, stirring rate, and liquid-to-solid (L/S) ratio on the mineralization of WS using simulated flue gas as the inlet. At 2 bars, the sequestration capacity is the lowest and steadily increases up to 259.8 g/kg throughout the 200-minute interval. Conversely, SC at 4 and 6 bars only differs at low reaction times and reaches the same maximum value after just 60 min (δCaO = 59.95 % and SC = 273 g_{CO2}/kg_{slag} at 4 bars, and δCaO = 61 % and SC = 277 g_{CO2}/kg_{slag} at 6 bars). These findings unveil reaction acceleration with increasing pressure. This phenomenon can be attributed to the increased dissolution of CO_2 in water, driven by the higher total gas pressure. Interestingly, despite the lower reaction kinetics, by reducing the pressure from 6 down to 2 bars, the maximum sequestration capacity remains similar. This demonstrates the potential of this mineralization process with WS for CO_2 capture from low-pressure steams such as flue gases. It's worth noting that reducing the total system pressure can help mitigate the energy consumption associated with the carbonation process, especially for these applications. Ultimately, we determined that the optimal conditions for the subsequent experiments were a pressure of 4 bars and a reaction time of 60 min.

In Fig. 3c, we show the effect of the liquid-to-solid ratio on the mineralization reaction. Carbon dioxide sequestration capacity increases by increasing the L/S ratio, reaching its maximum at 30 ml/g (SC = 330 g_{CO2}/kg_{slag}, δCaO = 73 %) and then decreasing. This observation contradicts previous work, where no significant influence of the L/S ratio in the mineralization reaction was found [48,64]. Our study shows a 35 % disparity in the SC value (330 compared to 215 g_{CO2}/kg_{slag}) at the 5–30 L/S ratio. The L/S ratio plays a crucial role in the mineralization reaction, influencing the alkalinity of the slurry and the ion leaching, thereby impacting the carbonation conversion [64,72]. Nonetheless, we opted for an L/S ratio of 20 ml/g for further analysis, considering that this value balances the amount of liquid and residue, as studied in previous works [25,40,41,45,46,48,61]. It is important to mention that while a higher solid/liquid ratio can result in a higher degree of carbonation, the amount of water to be treated also increases as a significant issue to be considered [72].

Since diffusion-controlled reactions govern accelerated mineralization, the influence of rotational speed on the carbonation efficiency was also investigated. The degree of carbonation increases with the rotation speed, reaching a maximum at 500 rpm and then decreasing at a higher speed (Fig. 3d). These results are in agreement with the literature, where it is reported that increasing the stirring rate moderately enhances the gas-phase mass transfer rate[73]. It is worth noting, however, that excessively high rotational speeds can concurrently diminish the gas residence time, subsequently lowering carbonation conversion[41]. The optimum stirring rate, 500 rpm in our reactor conditions, balances enhanced mass transfer and maintains an adequate residence time for optimal carbonation conversion.

The impact of the temperature on the mineralization reaction (Fig. 3e) reveals a decline in the sequestration capacity as temperature rises from 25 ºC to 80 ºC. The kinetics of calcium species dissolution can be accelerated by elevating the temperature. However, at high temperatures, the nucleation and growth of $CaCO_3$ might encounter impediments due to reduced CO_2 solubility, thus detrimentally affecting the carbonation reaction[47,74]. It is important to acknowledge that the liquid-to-solid ratio could also decrease within the reactor due to water evaporation at high temperatures and affecting the degree of carbonation. Prudent caution is thus advised when elevating the working temperature of carbonation in the solid-liquid phase to avert decreasing CO_2 sequestration performance. Conversely, mineralization in the solid-gas phase is conducted at significantly higher temperatures ranging from 500 to 650ºC[25].

Fig. 3f illustrates the pH measured at the end of the mineralization process for reaction times up to 200 min. The initial pH of the non-carbonated samples is notably high (ranging between 11.5 and 12.1) before experiencing an exponential decay over time, reaching pH 7.2 after 200 min. An increase in the total pressure of the gas mixture accelerates the reaction kinetics, resulting in a rapid pH decline. At pressures of 4 and 6 bar, the pH drops to 7 after 60 min compared to a pH 8.4 reached at 2 bar pressure. The pH monitoring serves as an indicative gauge of carbonation, as it influences both the dissolution of gaseous CO_2 and the leaching of calcium ions from the solid matrix of the slags. The dominant species in the slag slurry is carbonate (CO_3^{2-}) when the pH exceeds 10.3, while it shifts to bicarbonate (HCO^{3-}) in the 6.3–10.3 pH range. As carbonate plays a key role in the carbonation reaction, the effectiveness of carbonation diminishes with decreasing pH values[40,41,55]. Consequently, maintaining proper pH control is essential for

maximizing carbonation efficiency despite the added costs associated with the slag mineralization process. Furthermore, at the maximum carbonation capacity achieved using pure CO_2 gas (375 g_{CO2}/kg_{slag}), the corresponding pH value was 6.6. Since each experiment was replicated thrice to ensure reproducibility, we noted a 5 % deviation in the pH values. This discrepancy could be attributed to the pH measurements after the carbonation experiments. The interval required for reactor cooling and depressurization during this waiting period might have influenced the precision of the measurement. Continuous pH monitoring is recommended for optimal accuracy and enhanced carbonation capacity [41].

In the case of RWs, the carbonation reaction was significantly slower. The CO_2 mineralization reaction with RWs mixture at varying pressures (Fig. 4a) does not reach equilibrium even after 390 min (longest reaction time we analyzed). The maximum sequestration capacity (SC) observed is 311.87 g_{CO2}/kg_{slag}, with a nearly complete degree of carbonation (δCaO) of 96.45 %, achieved at 6 bar and 25 °C. The reaction's kinetics intensify with increasing CO_2 partial pressure. Moreover, we observe a rapid pH decay at 6 bar, stabilizing at 7.6 within 60 min (Figure S15). Conversely, at 2 bar and 4 bar, the pH decreases to a minimum of 7.6 after 390 min. A decline in sequestration capacity becomes evident as pressure decreases, with values of 259.25 g_{CO2}/kg_{slag} (δCaO = 80 %) and 159.39 g_{CO2}/kg_{slag} (δCaO = 49 %) observed at 4 bar and 2 bar, respectively.

The slower mineralization reaction kinetics in RWs are confirmed with the pH trend showing a gradual decrease (Figure S15), with a value of 9.5 after 60 min of reaction at 4 bar and 25 °C, the white slag reached pH 6.9 under same operating conditions (Fig. 3**f**). Nonetheless, rapid carbonation in the white slag, facilitated by its fast pH decay, leads to a swift obstruction of CO_2 sequestration in the slurry. Consequently, even at an operating pressure of 6 bar, the white slag achieves equilibrium in just 60 min, while the RWs do not reach equilibrium even after 390 min, with a difference of approximately 11 % discrepancy in sequestration capacity between these two residues, the RWs shows superior SC performance at longer reaction times. Moreover, RWs show a 36 % higher degree of carbonation than WS. The carbonate formation is directly proportional to the Ca and Mg silicate content, as delineated in Eq.1. Moreover, maintaining optimal pH levels is crucial for enhancing sequestration efficiency in SC. Rietveld analysis from the non-carbonated species (Tables S4 and S2) reveals that the White Slag (WS) contains a higher γ-Ca_2SiO_4 concentration (27.6 %) compared to the Refractory Wastes (RWs) at 18.8 %. This primary reactive agent in WS, accelerates pH reduction through rapid Ca+ ion release, thereby inhibiting the mineralization process due to a consequent decrease in carbonate ion (CO_3^{2-}) availability [5]. This is why WS shows considerable potential for enhanced carbon sequestration, evidenced by its δCaO content of 61 %, while RWs show almost complete carbonation.

The effect of temperature on the mineralization reaction at 2 bar pressure and 60 min (Fig. 4b) reveals a 26 % increase in SC (from 90 to 122 g_{CO2}/kg_{slag}) and δCaO (from 28 % to 38 %) when the temperature rises from 25 °C to 100 °C. This parameter warrants optimization for further application and confirms the positive influence of temperature on the carbonation kinetics in CO_2 mineralization using RWs. Fig. 4c compares the sequestration capacity and carbonation degree of WS, RWs, and individual components of RWs under the same operating conditions (4 bar, 25 °C, and 60 min). WS exhibits the highest SC at 271.7 g_{CO2}/kg_{slag} (with a δCaO = 59.9 %). Tundish RW demonstrates the highest carbonation degree (δCaO = 79.5 %), with a sequestration capacity of 163.7 g_{CO2}/kg_{slag}, exceeding the rest of refractory waste materials. Despite this, the δCaO value of Tundish RW suggests limited potential for further improvement in SC after longer reaction times.

3.3. Characterization of the carbonated solid and aqueous phases

Fig. 5 shows the SEM-XEDS results that illustrate the structural characteristics of both non and carbonated samples of WS and RWs along the elemental mapping. The morphological comparison of non-carbonated and carbonated WS (Fig. 5a-b) highlights an irregular-shaped non-carbonated sample and 2–3 μm cubic-shaped crystals ($CaCO_3$) due to slag carbonation. A continuous and compact layer of $CaCO_3$ crystals formed a continuous coating on the WS surface, consistent with the literature[69]. Elemental analysis indicates an increment in carbon content while not quantitatively significant. The corresponding elemental mapping (Fig. 5**c**) reveals a uniform Ca, O, C, and Si distribution through the sample. Minor elements such as Mg and S are present in focal points in the center of the sample. In contrast, elements like Mn, Al, Fe, Ti, and among others, exhibit irregular distribution through the carbonated sample (Figure S7c). Semi-quantitative XRD analysis (Fig. 6a) confirms the presence of $CaCO_3$ (calcite) as the primary mineral phase, with approximately 50 % in the carbonated WS. Comparative analysis of the main mineral phases reveals Ca_2SiO_4 as the initially predominant phase, which undergoes a substantial reduction, decreasing from approximately 49–18 %. The MgO remains mostly unchanged during carbonation, confirming its inertness. Several mineral phases identified in the non-carbonated WS, such as magnesian Gehlenite ($Ca_2Al_2SiO_7$) and Merwinite ($Ca_3Mg(SiO_4)_2$), are no longer present in the carbonated WS. Instead, novel mineral phases emerge, including Mayenite ($Ca_{12}Al_{14}O_{33}$), Hibschite ($Al_2Ca_3(SiO_4)_2$), and Wollastonite ($CaSiO_3$); for details refer to Figure S3a. FTIR analysis (Figure S14a) confirms the presence of characteristic C-O bonds associated with carbonate samples. The intense band centered at about 1409 cm^{-1} corresponds to the ν3 vibrations of CO_3^{-2} (asymmetric C–O stretching), while the peaks at 871 cm^{-1} and around 712 cm^{-1} are associated with out-plane and in-plane bending (ν2) vibrations of CO_3^{-2}, respectively [75–81]. The peak at 1795 cm^{-1} can also be ascribed to $CaCO_3$[80,82,83]. The increase in intensity of these bands for the carbonated WS sample confirms the calcite formation in white slag during the CO2 mineralization process.

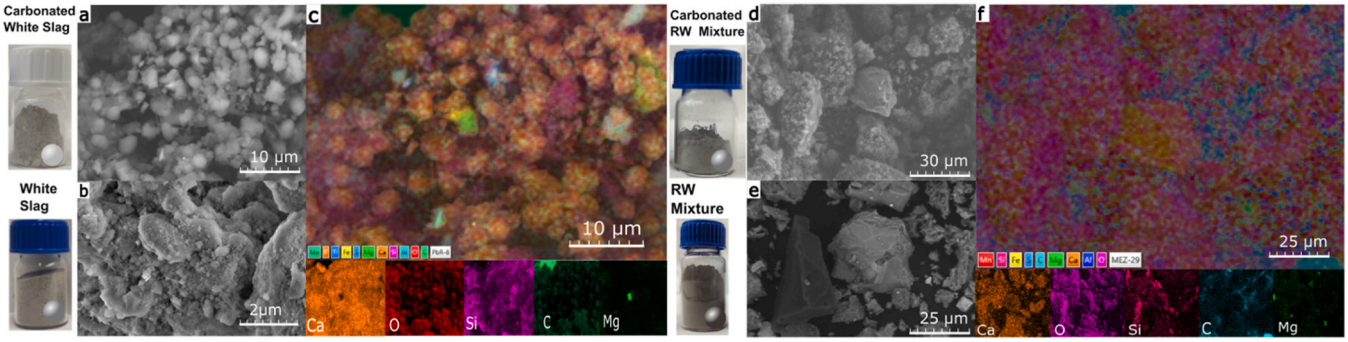

Fig. 5. Scanning electron micrographs (SEM) and elemental mapping of the carbonated samples of the white slag (a, c), the refractory wastes (d, f), and non-carbonated samples of WS and RWs (b and e, respectively).

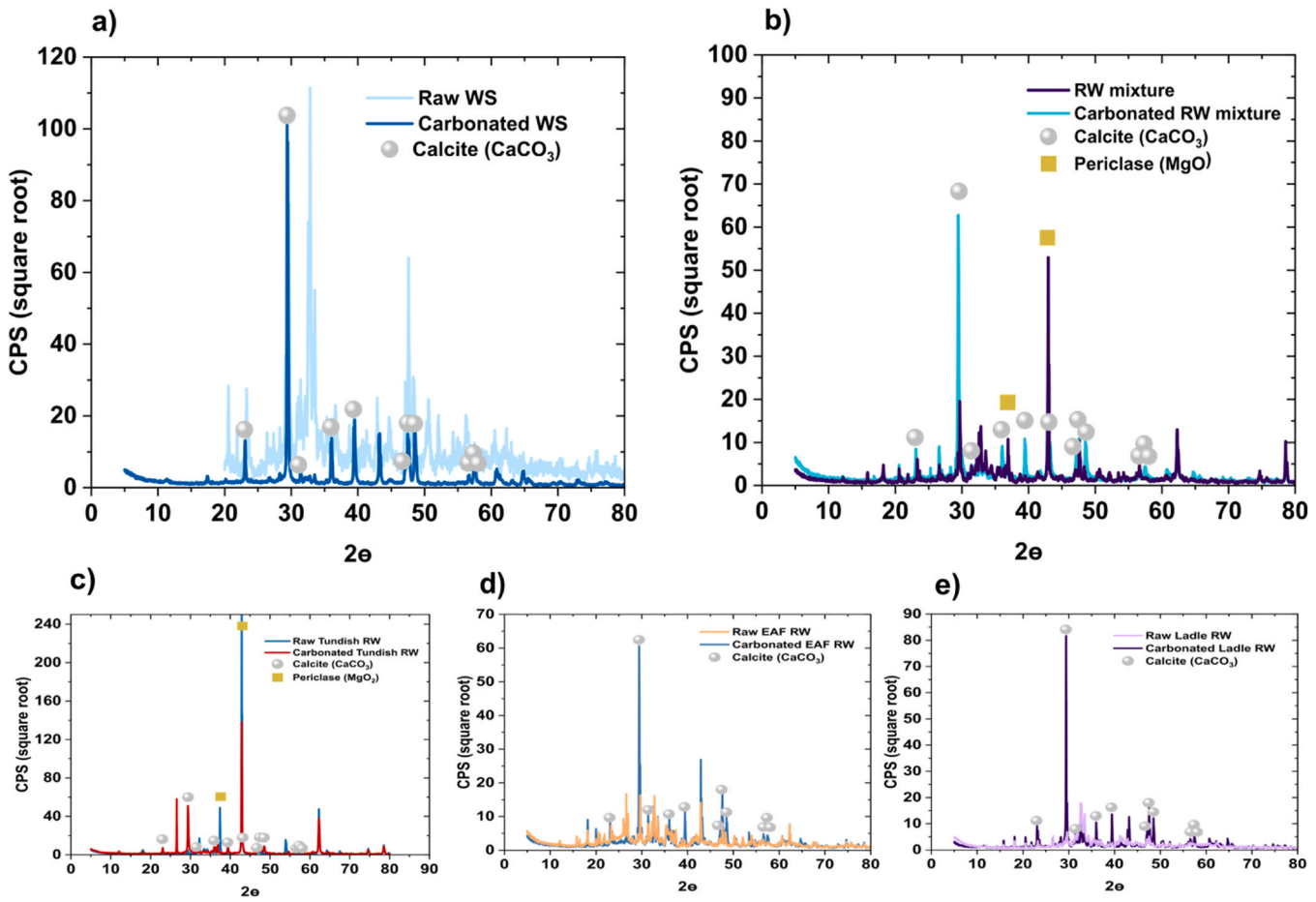

Fig. 6. XRD patterns of non-carbonated and carbonated samples of a) White Slag, b) RW mixture, c) Tundish RW, d) Electric Arc Furnace RW, and e) Ladle RW.

Morphological comparison of the non-carbonated and carbonated RWs mixture (Fig. 5d-e) reveals the formation of tiny calcite crystals adhering to the predominantly silicon-based particles following the mineralization process. RWs exhibits a more uniform elemental distribution (Fig. 5f) of the principal components such as Ca, Si, O, C, and Mg, primarily attributed to the homogenization step involving ball milling after mineralization. This homogenization step effectively addresses initial inconsistency in RWs carbonation, since, without it, the analytical results varied across different sampling points due to irregular carbonation throughout the sample (in contrast to the high homogeneity found in WS carbonation). Fig. 6b shows the XRD analysis for the non-carbonated and carbonated RWs. A distinct change in the intensity of active phases is observed, with calcite ($CaCO_3$) peaks intensifying and Ca_2SiO_4, in its mineral forms of larnite and olivine, either disappearing or exhibiting a partial reduction. Notably, in this case, MgO and Srebrodolskite ($Ca_2Fe_2O_5$) show no appreciable change. Conversely, mineral phases such as Bregidite ($Ca_{14}Mg_2(SiO_4)_8$), Enstatite ($MgSiO_3$), and Quartz (SiO_2) emerge in the carbonated RWs.

FTIR spectra (Figure S14b) reveals a change in the intensity of the bands in the 1400–1500 cm^{-1} range, typically attributed to asymmetric C–O stretching vibrations characteristic of carbonates. Additionally, peaks around 872 and 712 cm^{-1} are observed, corresponding to the out-of-plane and in-plane bending vibrations from trace carbonate-based compounds. These observations confirm the formation of $CaCO_3$ during carbonation. SEM, XRD, and FTIR analyses reveal the absence of $MgCO_3$ formation in the RWs. This underscores that the mineralization process can be exclusively attributed to the formation of Calcite. Furthermore, after the carbonation of each one of the individual RW, the morphological analysis (Figure S11) reveals the consistent formation of calcite layers enveloping solid particles, being more pronounced in the EAF RW and Ladle RW. Examining active mineral phases (Fig. 6c-e), calcium olivine ($CaSiO_4$) is the primary phase in the EAF RW and Ladle RW.

The analysis of the *aqueous phase* after the mineralization process is critical to understanding the effectiveness of the process. Previous studies[40,45,48,57,84] suggest that mineralization plays a fundamental role in preventing the leaching of heavy metals. Thus, it is essential to evaluate the composition of aqueous residues and explore the possibility of recycling them within the carbonation process[50]. In the case of WS (Figure S12), we observe a significant increase in the concentration of metallic ions in the early stages of the carbonation process, including Ti (reaching up to 56 μg/L), Al (reaching up to 1051 μg/L), Fe (reaching up to 64.5 μg/L), Ni (up to 5.5 μg/L) and Pb (reaching up to 612 μg/L). These metals leach in the liquid phase and disappear in the solid residues at short carbonation times. However, these metallic elements become trapped again within the solid matrix as part of the calcium oxides at longer reaction times. Their liquid phase concentration decreases to 10, 0.44, 46.2, and 7.5 μg/L for Ti, Al, Fe, and Pb, respectively. Ca, Mg, and to a lesser extent Cr and Ni, increase their concentration monotonically as the mineralization reaction progresses. At the 200 min reaction time, they reach 373, 274, 2.5, and 17.6 μg/L, respectively.

The concentration of Ca in RWs carbonation wastewater (Figure S13) peaks at 130 mg/L after 200 min, followed by a gradual decline. Similarly, Si exhibits a pronounced increase up to 200 min, followed by a slower growth rate with 92 mg/L after 390 min. Mg, Al, and Cr concentrations steadily increase with reaction time, reaching 2458 mg/L, 923 mg/L, and 13.5 μg/L after 390 min. Fe, Ti, and V show no

significant change up to 200 min but exhibit an exponential increase, reaching final values of 11.14, 666, and 57.6 μg/L, respectively. Pb concentration decreases exponentially after 60 min of reaction, reaching negligible levels (2 μg/L) by the end of the experiment. Furthermore, Figure S13i demonstrates that even at short reaction times, Pb concentration remains negligible (<3 μg/L) as the partial pressure of CO_2 increases. These analyses that confirm the minimum leaching found serve to ensure the potential interest of these mineralization protocols.

3.4. Outlook

The presence of free calcium oxide (free-CaO) and calcium hydroxide ($Ca(OH)_2$) in steel slag typically hinders its application in concrete, asphalt aggregate, road base, and fill materials due to associated issues with water absorption and expansion[45]. Carbonation treatment eliminates reactive calcium-rich components (e.g., free-CaO, $Ca(OH)_2$, Ca_2SiO_4) from White Slag and Refractory Wastes, making them safer and more sustainable. The sequestration capacities (SC) and carbonation degrees (δCaO) reported in this study fall within the range reported in the existing literature. Using pure CO_2 gas, the δCaO ranges from 53 % to 86 %, while 20–30 % CO_2 gas mixtures produce δCaO between 28 % and 57 % [22,25,32,40,54,57]. This study is focused on flue gases with lower CO_2 concentrations, diverging from prevalent studies centered on higher CO_2 concentrations typical of blast furnace emissions[32].

Moreover, our study introduces Refractory Wastes (RWs) as carbon capture materials exhibiting high conversion rates (96 %) under extended carbonation reaction times, marking a significant area for subsequent inquiry. Future research should focus on detailed, source-specific investigations to effectively manage and utilize slag waste in mineralization processes. It is essential to thoroughly validate the corresponding carbonated residues to confirm their efficiency as alternative materials in construction, which will encourage their wider use.

While our study has advanced our comprehension of the mineralization process in steelmaking wastes (white slag and refractories waste), several perspectives warrant exploration to develop a more comprehensive approach to managing these wastes through mineralization. These perspectives and avenues for future research encompass a*) Rigorous Techno-Economic Analysis*: Conducting an exhaustive techno-economic analysis is imperative. This should contain diverse scenarios and models for circular economic integration with complementary industries. By quantifying costs, energy inputs, and potential savings, such an analysis will provide a clearer picture of the economic feasibility and sustainability of waste mineralization. *b) Leaching Studies for Heavy Metal Stabilization:* Further investigations into leaching are essential to validate the effectiveness of mineralization in stabilizing heavy metals within the solid carbonate residue. This research is pivotal for understanding the long-term environmental implications and safety of carbonated waste material. Finally, a *c) Validation of Carbonated Wastes as Construction Material Additives:* Robust validation studies are required to ascertain the viability of utilizing carbonated waste materials as additives for construction materials. This exploration could potentially lead to the development of sustainable and environmentally friendly construction practices. By addressing these crucial aspects, future work can contribute to advancing waste mineralization and its integration into a broader sustainable industrial ecosystem.

4. Conclusions

Mineralization offers a promising pathway to simultaneously address CO_2 emissions and the valorization of high-basicity waste materials, demonstrating the feasibility of a unified CO_2 capture and storage approach using industry byproducts, and promoting circular economy principles. Our study introduces a comprehensive approach focused on the mineralization of both White Slag (WS), along with Refractory Wastes (RWs) from electric arc furnace, ladle furnace, and tundish, highlighting their untapped potential within the secondary steel industry.

Carbonated White Slag achieved a peak CO_2 sequestration capacity of 276.65 gCO_2/kg_{slag} (10 % CO_2 gas mixture) and 359.79 gCO_2/kg_{slag} (pure CO_2). These results highlight the potential for direct mineralization using rolling mill furnace off-gases, eliminating the need for energy-intensive CO_2 pre-concentration step.

Optimization studies revealed peak performance for WS at 60 min, 4 bar, 25 °C, and a liquid-to-solid ratio of 20 (271.67 $gCO_2\ kg_{slag}$). RWs, while exhibiting slower kinetics, reached a higher maximum of 311 gCO_2/kg_{slag} after 390 min. Additionally, Tundish RW showed the highest carbonation degree (79 %) and CO_2 sequestration capacity (165 gCO_2/kg_{slag}) among the individual RW fractions. Furthermore, solution pH plays a critical role in the mineralization reaction, and strategies to control pH during the mineralization process warrant further investigation.

Characterization studies (SEM, XRD, TGA, FTIR, and ICP) confirmed CaO as the primary reactant in the mineralization process, while MgO remained essentially inert in these conditions. Only structural and mineralogical changes in calcic compounds were detected.

Addressing environmental concerns, particularly for Tundish RW because of its higher Pb content, our findings suggest that the carbonation process may also stabilize heavy metals like Pb. Reduced Pb concentration in filtrated water as the mineralization reaction progresses indicates that harmful metals could be trapped within the carbonated material. This warrants further investigation as a potential waste remediation strategy.

In summary, our results demonstrates the potential of mineralization to address both CO_2 emissions and a wide range of waste streams within the steel industry, contributing to sustainable industrial ecology. The successful use of the steel industry off-gas emphasizes the potential for immediate implementation and emissions reduction. Additionally, stabilizing heavy metals in carbonated material presents a promising approach for future innovations in waste management.

CRediT authorship contribution statement

José Ramón Galán-Mascaros: Writing – review & editing, Supervision, Funding acquisition. **Anna Casals-Terré:** Supervision, Funding acquisition. **Stefano Giancola:** Writing – review & editing, Supervision. **Raiana Tomazini de Oliveira:** Methodology, Investigation, Data curation. **Santiago Capelo-Avilés:** Writing – original draft, Supervision, Project administration, Investigation, Funding acquisition, Data curation, Conceptualization. **Francesc Gispert-Guirado:** Investigation, Data curation. **Irene Isabel Gallo Stampino:** Methodology, Investigation, Data curation.

Declaration of Competing Interest

We declare no conflict of interest.

Data availability

Data will be made available on request.

Acknowledgments

We acknowledge the financial support from MCIN/AEI through projects PID2021-124796OB-I00 and PDC2022-133214-I00; and from the Generalitat de Catalunya (2021SGR1154). ICIQ is supported by the Ministerio de Ciencia e Innovación through the Severo Ochoa Excellence Accreditations CEX2019-000925-S (MCIN/AEI) and CEX2021-001214-S; and by the CERCA Programme/Generalitat de Catalunya. S.G.A. thanks AGAUR for a PhD industrial fellowship (2019 DI 73).

Appendix A. Supporting information

Supplementary data associated with this article can be found in the online version at doi:10.1016/j.jcou.2024.102770.

References

[1] IEAEnergy Efficiency Indicators Highlights International Energy Agency , 2018, 191, 10.1080/10511482.1993.9521135.

[2] T.A. Kurniawan, M.H.D. Othman, X. Liang, H.H. Goh, P. Gikas, T.D. Kusworo, A. Anouzla, K.W. Chew, Decarbonization in waste recycling industry using digitalization to promote net-zero emissions and its implications on sustainability, J. Environ. Manag. 338 (2023) 117765, https://doi.org/10.1016/j.jenvman.2023.117765.

[3] C. DiGiovanni, O.A. Hisseine, A.N. Awolayo, Carbon dioxide sequestration through steel slag carbonation: review of mechanisms, process parameters, and cleaner upcycling pathways, J. CO2 Util. 81 (2024) 102736, https://doi.org/10.1016/j.jcou.2024.102736.

[4] W. Liu, L. Teng, S. Rohani, Z. Qin, B. Zhao, C.C. Xu, S. Ren, Q. Liu, B. Liang, CO2 mineral carbonation using industrial solid wastes: a review of recent developments, Chem. Eng. J. 416 (2021) 129093, https://doi.org/10.1016/j.cej.2021.129093.

[5] H. Xie, H. Yue, J. Zhu, B. Liang, C. Li, Y. Wang, L. Xie, X. Zhou, Scientific and engineering progress in CO2 mineralization using industrial waste and natural minerals, Proc. Est. Acad. Sci. Eng. 1 (2015) 150–157, https://doi.org/10.15302/J-ENG-2015017.

[6] Y. Yoo, I. Kim, D. Lee, W. Yong Choi, J. Choi, K. Jang, J. Park, D. Kang, Review of contemporary research on inorganic CO2 utilization via CO2 conversion into metal carbonate-based materials, J. Ind. Eng. Chem. 116 (2022) 60–74, https://doi.org/10.1016/j.jiec.2022.09.007.

[7] Z. Chen, Z. Cang, F. Yang, J. Zhang, L. Zhang, Carbonation of steelmaking slag presents an opportunity for carbon neutral: a review, J. CO2 Util. 54 (2021) 101738, https://doi.org/10.1016/j.jcou.2021.101738.

[8] S. Srivastava, R. Snellings, P. Nielsen, P. Cool, Insights into CO2-mineralization using non-ferrous metallurgy slags: CO2(g)-induced dissolution behavior of copper and lead slags, J. Environ. Chem. Eng. 10 (2022) 107338, https://doi.org/10.1016/j.jece.2022.107338.

[9] H. Ostovari, L. Müller, J. Skocek, A. Bardow, From unavoidable CO2 source to CO2 sink? A cement industry based on CO2 mineralization, Environ. Sci. Technol. 55 (2021) 5212–5223, https://doi.org/10.1021/acs.est.0c07599.

[10] S. Tanaka, K. Takahashi, M. Abe, M. Noguchi, A. Yamasaki, Preparation of high-purity calcium carbonate by mineral carbonation using concrete sludge, ACS Omega 7 (2022) 19600–19605, https://doi.org/10.1021/acsomega.2c01297.

[11] F.M. Kusin, S.N.M.S. Hasan, V.L.M. Molahid, F.M. Yusuff, S. Jusop, Carbon dioxide sequestration of iron ore mining waste under low-reaction condition of a direct mineral carbonation process, Environ. Sci. Pollut. Res. Int. 30 (2023) 22188–22210, https://doi.org/10.1007/s11356-022-23677-3.

[12] M. Hanifa, R. Agarwal, U. Sharma, P.C. Thapliyal, L.P. Singh, A review on CO2 capture and sequestration in the construction industry: emerging approaches and commercialised technologies, J. CO2 Util. 67 (2023) 102292, https://doi.org/10.1016/j.jcou.2022.102292.

[13] T. Zhang, M. Chen, Y. Wang, M. Zhang, Roles of carbonated recycled fines and aggregates in hydration, microstructure and mechanical properties of concrete: a critical review, Cem. Concr. Compos. 138 (2023) 104994, https://doi.org/10.1016/j.cemconcomp.2023.104994.

[14] L. Li, Q. Liu, T. Huang, W. Peng, Mineralization and utilization of CO2 in construction and demolition wastes recycling for building materials: a systematic review of recycled concrete aggregate and recycled hardened cement powder, Sep. Purif. Technol. 298 (2022) 121512, https://doi.org/10.1016/j.seppur.2022.121512.

[15] Z. Li, Y. Xing, M. Ma, W. Su, Y. Cui, J. Tian, F. Fei, Towards the co-benefits of carbon capture, utilization and sequestration: a life cycle assessment study for steel slag disposal, J. Clean. Prod. 443 (2024) 141166, https://doi.org/10.1016/j.jclepro.2024.141166.

[16] P. Bakshi, A. Pappu, D.K. Bharti, B. Parmar, R. Patidar, A.K. Srivastava, Life cycle assessment of calcium-rich industrial waste reinforced polypropylene and low-density polyethylene composites using the cradle-to-gate approach, ACS Sustain. Chem. Eng. 10 (2022) 13710–13721, https://doi.org/10.1021/acssuschemeng.2c03751.

[17] L. Li, T.-C. Ling, S.-Y. Pan, Environmental benefit assessment of steel slag utilization and carbonation: a systematic review, Sci. Total Environ. 806 (2022) 150280, https://doi.org/10.1016/j.scitotenv.2021.150280.

[18] L. Li, Y. Jiang, S.-Y. Pan, T.-C. Ling, Comparative life cycle assessment to maximize CO2 sequestration of steel slag products, Constr. Build. Mater. 298 (2021) 123876, https://doi.org/10.1016/j.conbuildmat.2021.123876.

[19] D. Stefaniuk, M. Hajduczek, J.C. Weaver, F.J. Ulm, A. Masic, Cementing CO2 into C-S-H: A step toward concrete carbon neutrality, PNAS Nexus 2 (2023) gad052, https://doi.org/10.1093/pnasnexus/pgad052.

[20] H. Ostovari, L. Müller, F. Mayer, A. Bardow, A climate-optimal supply chain for CO2 capture, utilization, and storage by mineralization, J. Clean. Prod. 360 (2022) 131750, https://doi.org/10.1016/j.jclepro.2022.131750.

[21] G. Hu, S. Rohani, X. Jiang, J. Li, Q. Liu, W. Liu, CO2 mineral sequestration and faujasite zeolite synthesis by using blast furnace slag: process optimization and CO2 net-emission reduction evaluation, ACS Sustain. Chem. Eng. 9 (2021) 13963–13971, https://doi.org/10.1021/acssuschemeng.1c05576.

[22] S.-Y. Pan, Y.-H. Chen, L.-S. Fan, H. Kim, X. Gao, T.-C. Ling, P.-C. Chiang, S.-L. Pei, G. Gu, CO2 mineralization and utilization by alkaline solid wastes for potential carbon reduction, Nat. Sustain. 3 (2020) 399–405, https://doi.org/10.1038/s41893-020-0486-9.

[23] R. Ragipani, K. Sreenivasan, R.P. Anex, H. Zhai, B. Wang, Direct air capture and sequestration of CO2 by accelerated indirect aqueous mineral carbonation under ambient conditions, ACS Sustain. Chem. Eng. 10 (2022) 7852–7861, https://doi.org/10.1021/acssuschemeng.1c07867.

[24] Global Renewables Outlook 2020, IRENA, 2020. ⟨https://www.irena.org/-/media/Files/IRENA/Agency/Publication/2020/Apr/IRENA_Global_Renewables_Outlook_2020.pdf⟩.

[25] Y. Zhang, L. Yu, K. Cui, H. Wang, T. Fu, Carbon capture and storage technology by steel-making slags: recent progress and future challenges, Chem. Eng. J. 455 (2023) 140552, https://doi.org/10.1016/j.cej.2022.140552.

[26] Global Warming of 1.5 oC, (n.d.). ⟨https://www.ipcc.ch/sr15/⟩. (accessed August 29, 2023).

[27] International Energy Agency, An updated roadmap to Net Zero Emissions by 2050, in: World Energy Outlook, Organisation for Economic Co-operation and Development, 2022. https://doi.org/10.1787/afc95219-en.

[28] International Energy AgencyThe ambition gap to 1.5 °C, in: world energy Outlook OECD , 2021, 10.1787/60841dca-en.

[29] J. Xie, Z. Xia, X. Tian, Y. Liu, Nexus and synergy between the low-carbon economy and circular economy: A systematic and critical review, Environ. Impact Assess. Rev. 100 (2023) 107077, https://doi.org/10.1016/j.eiar.2023.107077.

[30] Steel - The permanent material in the circular economy, Worldsteel.org (2021). ⟨https://worldsteel.org/circulareconomy/⟩ (accessed August 2023).

[31] Q. Zhao, X. Chu, X. Mei, Q. Meng, J. Li, C. Liu, H. Saxén, R. Zevenhoven, Co-treatment of waste from steelmaking processes: steel slag-based carbon capture and storage by mineralization, Front. Chem. 8 (2020) 1–7, https://doi.org/10.3389/fchem.2020.571504.

[32] Z. Yi, T. Wang, R. Guo, Sustainable building material from CO2mineralization slag: aggregate for concretes and effect of CO2curing, J. CO2 Util. 40 (2020) 101196, https://doi.org/10.1016/j.jcou.2020.101196.

[33] H. Li, Z. Tang, N. Li, L. Cui, X.-Z. Mao, Mechanism and process study on steel slag enhancement for CO2 capture by seawater, Appl. Energy 276 (2020) 115515, https://doi.org/10.1016/j.apenergy.2020.115515.

[34] S. Yadav, A. Mehra, A review on ex situ mineral carbonation, Environ. Sci. Pollut. Res. 28 (2021) 12202–12231, https://doi.org/10.1007/s11356-020-12049-4.

[35] S.Y. Pan, E.E. Chang, P.C. Chiang, CO2 capture by accelerated carbonation of alkaline wastes: a review on its principles and applications, Aerosol Air Qual. Res. 12 (2012) 770–791, https://doi.org/10.4209/aaqr.2012.06.0149.

[36] S.C. Tian, J.G. Jiang, K.M. Li, F. Yan, X.J. Chen, Performance of steel slag in carbonation-calcination looping for CO 2 capture from industrial flue gas, RSC Adv. 4 (2014) 6858–6862, https://doi.org/10.1039/c3ra47426g.

[37] M.T. Vu, L.N. Nguyen, I. Ibrahim, M. Abu Hasan Johir, N. Bich Hoang, X. Zhang, L. D. Nghiem, Nutrient recovery from digested sludge centrate using alkali metals from steel-making slag, Chem. Eng. J. 450 (2022) 138186, https://doi.org/10.1016/j.cej.2022.138186.

[38] H. Yi, G. Xu, H. Cheng, J. Wang, Y. Wan, H. Chen, An overview of utilization of steel slag, Procedia Environ. Sci. 16 (2012) 791–801, https://doi.org/10.1016/j.proenv.2012.10.108.

[39] B. Zeng, Z. Zhang, S. Yang, L. Mo, F. Jin, Alkanolamines-activated steel slag for stabilization/solidification of heavy metal contaminated soil, J. Environ. Chem. Eng. 11 (2023) 110301, https://doi.org/10.1016/j.jece.2023.110301.

[40] Pen-Chi Chiang, Shu-Yuan Pan. Carbon Dioxide Mineralization and Utilization, first ed., Springer, Singapore, 2017. ⟨https://link.springer.com/book/10.1007/978-981-10-3268-4⟩.

[41] S.Y. Pan, T.C. Chung, C.C. Ho, C.J. Hou, Y.H. Chen, P.C. Chiang, CO2 mineralization and utilization using steel slag for establishing a waste-to-resource supply chain, Sci. Rep. 7 (2017) 1–11, https://doi.org/10.1038/s41598-017-17648-9.

[42] A. Ebrahimi, M. Saffari, D. Milani, A. Montoya, M. Valix, A. Abbas, Sustainable transformation of fly ash industrial waste into a construction cement blend via CO2 carbonation, J. Clean. Prod. 156 (2017) 660–669, https://doi.org/10.1016/j.jclepro.2017.04.037.

[43] A. Di Maria, R. Snellings, L. Alaerts, M. Quaghebeur, K. Van Acker, Environmental assessment of CO2 mineralisation for sustainable construction materials, Int. J. Greenh. Gas. Control 93 (2020) 102882, https://doi.org/10.1016/j.ijggc.2019.102882.

[44] Y. Du, C. Fu, B. Gong, E. Miao, X. Zheng, Z. Xiong, Y. Zhao, J. Zhang, Real-time investigation of the CO2 mineral carbonation reaction rate through direct aqueous route using semi-dry desulfurization slag, J. CO2 Util. 51 (2021) 101614, https://doi.org/10.1016/j.jcou.2021.101614.

[45] S.Y. Pan, P.C. Chiang, Y.H. Chen, C.S. Tan, E.E. Chang, Ex Situ CO2 capture by carbonation of steelmaking slag coupled with metalworking wastewater in a rotating packed bed, Environ. Sci. Technol. 47 (2013) 3308–3315, https://doi.org/10.1021/es304975y.

[46] E.-E. Chang, C.-H. Chen, Y.-H. Chen, S.-Y. Pan, P.-C. Chiang, Performance evaluation for carbonation of steel-making slags in a slurry reactor, 02/, J. Hazard. Mater. 186 (2011) 558–564, https://doi.org/10.1016/j.jhazmat.2010.11.038.

[47] E.E. Chang, S.Y. Pan, Y.H. Chen, C.S. Tan, P.C. Chiang, Accelerated carbonation of steelmaking slags in a high-gravity rotating packed bed, J. Hazard. Mater. 227–228 (2012) 97–106, https://doi.org/10.1016/j.jhazmat.2012.05.021.

[48] E.-E. Chang, S.-Y. Pan, Y.-H. Chen, H.-W. Chu, C.-F. Wang, P.-C. Chiang, CO2 sequestration by carbonation of steelmaking slags in an autoclave reactor, 11/,

J. Hazard. Mater. 195 (2011) 107–114, https://doi.org/10.1016/j.jhazmat.2011.08.006.
[49] H. Yan, G. Zhang, Y. Wang, J. Liu, G. Li, Y. Zhao, Y. Xu, Y. Lv, A green synthesis strategy for low-cost multi-porous solid CO2 adsorbent using blast furnace slag, 12/, Fuel 329 (2022) 125380, https://doi.org/10.1016/j.fuel.2022.125380.
[50] J. Lee, K.H. Ryu, H.Y. Ha, K.D. Jung, J.H. Lee, Techno-economic and environmental evaluation of nano calcium carbonate production utilizing the steel slag, J. CO2 Util. 37 (2020) 113–121, https://doi.org/10.1016/j.jcou.2019.12.005.
[51] S. Srivastava, M. Cerutti, H. Nguyen, V. Carvelli, P. Kinnunen, M. Illikainen, Carbonated steel slags as supplementary cementitious materials: reaction kinetics and phase evolution, Cem. Concr. Compos. 142 (2023) 105213, https://doi.org/10.1016/j.cemconcomp.2023.105213.
[52] P. Liu, L. Mo, J. Zhong, M. Tang, In-situ investigation on the carbonation behaviors of various mineral phases in steel slag: the role of RO phase, Cem. Concr. Compos. 149 (2024) 105524, https://doi.org/10.1016/j.cemconcomp.2024.105524.
[53] A. Sanna, M. Uibu, G. Caramanna, R. Kuusik, M.M. Maroto-Valer, A review of mineral carbonation technologies to sequester CO2, Chem. Soc. Rev. 43 (2014) 8049–8080, https://doi.org/10.1039/c4cs00035h.
[54] K.R. Reddy, A. Gopakumar, J.K. Chetri, Critical review of applications of iron and steel slags for carbon sequestration and environmental remediation, Rev. Environ. Sci. Technol. 18 (2019) 127–152, https://doi.org/10.1007/s11157-018-09490-w.
[55] A. Azdarpour, M. Asadullah, E. Mohammadian, H. Hamidi, R. Junin, M.A. Karaei, A review on carbon dioxide mineral carbonation through pH-swing process, Chem. Eng. J. 279 (2015) 615–630, https://doi.org/10.1016/j.cej.2015.05.064.
[56] M. Liu, A. Hohenshil, G. Gadikota, Integrated CO $_2$ capture and removal via carbon mineralization with inherent regeneration of aqueous solvents, Energy Fuels 35 (2021) 8051–8068, https://doi.org/10.1021/acs.energyfuels.0c04346.
[57] P. Renforth, The negative emission potential of alkaline materials, Nat. Commun. 10 (2019), https://doi.org/10.1038/s41467-019-09475-5.
[58] W.J.J. Huijgen, G.J. Witkamp, R.N.J. Comans, Mineral CO2 sequestration by steel slag carbonation, Environ. Sci. Technol. 39 (2005) 9676–9682, https://doi.org/10.1021/es050795f.
[59] K.S. Lackner, A guide to CO2 sequestration, Science 300 (2003) 1677–1678, https://doi.org/10.1126/science.1079033.
[60] W.J.J. Huijgen, R.N.J. Comans, Carbonation of steel slag for CO2 sequestration: Leaching of products and reaction mechanisms, Environ. Sci. Technol. 40 (2006) 2790–2796, https://doi.org/10.1021/es052534b.
[61] J. Gao, C. Li, W. Liu, J. Hu, L. Wang, Q. Liu, B. Liang, H. Yue, G. Zhang, D. Luo, S. Tang, Process simulation and energy integration in the mineral carbonation of blast furnace slag, Chin. J. Chem. Eng. 27 (2019) 157–167, https://doi.org/10.1016/j.cjche.2018.04.012.
[62] S.-I. Jo, Y.-I. An, K.-Y. Kim, S.-Y. Choi, J.-S. Kwak, K.-R. Oh, Y.-U. Kwon, Mechanisms of absorption and desorption of CO2 by molten NaNO3-promoted MgO, Phys. Chem. Chem. Phys. 19 (2017) 6224–6232, https://doi.org/10.1039/c6cp07787k.
[63] S.J. Gregg, J.D. Ramsay, Adsorption of Carbon Dioxide by Magnesia studied by Use of Infrared and Isotherm Measurements, (n.d.). https://doi.org/10.1039/J19700002784.
[64] T.-L. Chen, S.-L. Pei, P.-C. Chiang, Integrated leaching–carbonation kinetic model on CO $_2$ mineralization of alkaline solid wastes in a high-gravity rotating packed bed, React. Chem. Eng. 5 (2020) 1929–1938, https://doi.org/10.1039/D0RE00239A.
[65] H.M. Rietveld, A profile refinement method for nuclear and magnetic structures, J. Appl. Crystallogr. 2 (1969) 65–71, https://doi.org/10.1107/S0021889869006558.
[66] R.W. Cheary, A.A. Coelho, J.P. Cline, Fundamental Parameters Line Profile Fitting in Laboratory Diffractometers Volume 109 Number 1 January-February 2004, (n.d.). ⟨https://nvlpubs.nist.gov/nistpubs/jres/109/1/j91che.pdf⟩.
[67] R.J. Hill, C.J. Howard, Quantitative phase analysis from neutron powder diffraction data using the Rietveld method, J. Appl. Crystallogr. 20 (1987) 467–474, https://doi.org/10.1107/s0021889887086199.
[68] A.R. Stokes, A.J.C. Wilson, A method of calculating the integral breadths of Debye-Scherrer lines, Math. Proc. Camb. Philos. Soc. 38 (1942) 313–322, https://doi.org/10.1017/s0305004100021988.
[69] D. Wang, C. Xiong, W. Li, J. Chang, Growth of calcium carbonate induced by accelerated carbonation of tricalcium silicate, ACS Sustain. Chem. Eng. 8 (2020) 14718–14731, https://doi.org/10.1021/acssuschemeng.0c02260.
[70] J. Chang, Y. Fang, Quantitative analysis of accelerated carbonation products of the synthetic calcium silicate hydrate(C–S–H) by QXRD and TG/MS, 1/, J. Therm. Anal. Calorim. 119 (2015) 57–62, https://doi.org/10.1007/s10973-014-4093-8.
[71] S. Hong, S. Moon, J. Cho, A.-H.A. Park, Y. Park, Effects of Mg ions on the structural transformation of calcium carbonate and their implication for the tailor-synthesized carbon mineralization process, J. CO2 Util. 60 (2022) 101999, https://doi.org/10.1016/j.jcou.2022.101999.
[72] W.J.J. Huijgen, G.J. Ruijg, R.N.J. Comans, G.J. Witkamp, Energy consumption and net CO2 sequestration of aqueous mineral carbonation, Ind. Eng. Chem. Res. 45 (2006) 9184–9194, https://doi.org/10.1021/ie060636k.
[73] Y.H. Chen, C.Y. Chang, W.L. Su, C.C. Chen, C.Y. Chiu, Y.H. Yu, P.C. Chiang, S.I. M. Chiang, Modeling ozone contacting process in a rotating packed bed, Ind. Eng. Chem. Res. 43 (2004) 228–236, https://doi.org/10.1021/ie030545c.
[74] S.-Y. Pan, P.-C. Chiang, Y.-H. Chen, C.-D. Chen, H.-Y. Lin, E.-E. Chang, Systematic approach to determination of maximum achievable capture capacity via leaching and carbonation processes for alkaline steelmaking wastes in a rotating packed bed, Environ. Sci. Technol. 47 (2013) 13677–13685, https://doi.org/10.1021/es403323x.
[75] P. Kuśtrowski, L. Chmielarz, E. Bożek, M. Sawalha, F. Roessner, Acidity and basicity of hydrotalcite derived mixed Mg–Al oxides studied by test reaction of MBOH conversion and temperature programmed desorption of NH3 and CO2, 2/, Mater. Res. Bull. 39 (2004) 263–281, https://doi.org/10.1016/j.materresbull.2003.09.032.
[76] L. Fernandez, C. Alonso, A. Hidalgo, C. Andrade, The role of magnesium during the hydration of C3S and C-S-H formation. Scanning electron microscopy and mid-infrared studies, Adv. Cem. Res. (2015), https://doi.org/10.1680/adcr.2005.17.1.9.
[77] P. Yu, R.J. Kirkpatrick, B. Poe, P.F. McMillan, X. Cong, Structure of calcium silicate hydrate (C-S-H): near-, mid-, and far-infrared spectroscopy, J. Am. Ceram. Soc. 82 (1999) 742–748, https://doi.org/10.1111/j.1151-2916.1999.tb01826.x.
[78] J.T. Kloprogge, R.L. Frost, Fourier transform infrared and raman spectroscopic study of the local structure of Mg-, Ni-, and Co-hydrotalcites, J. Solid State Chem. 146 (1999) 506–515, https://doi.org/10.1006/jssc.1999.8413.
[79] H. Aguiar, J. Serra, P. González, B. León, Structural study of sol–gel silicate glasses by IR and Raman spectroscopies, J. Non-Cryst. Solids 355 (2009) 475–480, https://doi.org/10.1016/j.jnoncrysol.2009.01.010.
[80] A.I. Cadiș, F.Ștefania Rus, J.N. Gonçalves, M. Ivanovici, Preparing a Ca-Bi-O system by the precipitation method and studying its intermediate structural properties for applications in water treatment, /2, Inorganics 11 (2023) 79, https://doi.org/10.3390/inorganics11020079.
[81] A. Meiszterics, L. Rosta, H. Peterlik, J. Rohonczy, S. Kubuki, P. Henits, K. Sinkó, Structural characterization of gel-derived calcium silicate systems, J. Phys. Chem. A 114 (2010) 10403–10411, https://doi.org/10.1021/jp1053502.
[82] A.G. Xyla, P.G. Koutsoukos, Quantitative analysis of calcium carbonate polymorphs by infrared spectroscopy, J. Chem. Soc. Lond. Faraday Trans. 85 (1) (1989) 3165, https://doi.org/10.1039/f19898503165.
[83] J. Kiefer, A. Stärk, A.L. Kiefer, H. Glade, Infrared SPectroscopic Analysis of the Inorganic Deposits from Water in Domestic and Technical Heat Exchangers, /4, Energies 11 (2018) 798, https://doi.org/10.3390/en11040798.
[84] H.-J. Ho, A. Iizuka, H. Kubo, Direct aqueous carbonation of dephosphorization slag under mild conditions for CO2 sequestration and utilization: exploration of new dephosphorization slag utilization, Environ. Technol. Innov. 28 (2022) 102905, https://doi.org/10.1016/j.eti.2022.102905.

Santiago Capelo Avilés, a chemical engineer specializing in sustainable industrial processes, is pursuing an industrial doctorate at the Chemical Research Institute of Catalonia (ICIQ) in collaboration with steel manufacturer Compañia Española de Laminación S.L. (CELSA). With a Master's in Thermodynamic Engineering of Fluids from Rovira i Virgili University (URV), he previously contributed to applied thermal engineering research within the CREVER group. His expertise encompasses sustainable process design, emphasizing energy production, optimization, and carbon capture technologies. He has a deep knowledge of various industrial structures acquired from his active participation in numerous green power generation innovation projects at European and national level.

Raiana Tomazini de Oliveira, a laboratory technician at the Chemical Research Institute of Catalonia (ICIQ), is pursuing a Ph.D. in Chemical Science and Technology at Rovira i Virgili University (URV). She earned her chemical engineering degree from Fluminense Federal University (UFF) in Brazil, including an exchange program at URV. With a master's from the Alberto Luiz Coimbra Institute for Graduate Studies and Research in Engineering (COPPE) at the Federal University of Rio de Janeiro, Raiana specializes in recycling plastic waste and biomass for fuel production and heterogeneous catalysis. Her expertise extends to industrial CO2 capture and valorization projects, highlighting a diverse and impactful research background.

Irene Gallo Stampino serves ats laboratory technician at Institute of Chemical Research of Catalonia (ICIQ). She studied Chemical Engineering at Universidad de Zaragoza and did a stay in Technical University of Denmark (DTU), in which she realized her bachelor project. After this, she worked in companies related with the petroleum field.

Francesc Gispert-Guirado is Graduated of Geological Sciences by the University of Barcelona (1991) and obtained his Ph.D. at the same university in the Department of Crystallography (1998). He is the responsible of the X-ray Diffraction laboratory of the Scientific Resources Service (SRCiT) at the University Rovira I Virgili (Tarragona, Spain), since 1996. He is specialized on quantitative phase analysis and profile analysis from X-ray diffraction data using the software TOPAS (Bruker AXS), developing specific routines for solving crystallographic problems. Has published several papers related with these topics in journals of crystallography, materials and catalysis (ORCID 0000–0001–9553–2023).

Ms. Anna Casals Terre, is an Industrial Engineer with a Master's in Project Management from the Polytechnic University of Catalonia (UPC). As an Assistant Professor at UPC's Mechanical Engineering Department, she guided numerous thesis projects. She worked as a technology promoter at the EURECAT Foundation Technology Centre of Catalonia, leading and managing R+D+I projects. Her focus included the development of new materials, new manufacturing processes, robotics, and sustainability. Currently, as the Innovation Head of CELSA Spain and France Group, she shapes the R&D strategy, overseeing projects in sustainability and circular economy, material science, and digitalization within the steel industry. Her role extends to managing Innovation and CAPEX funding, providing crucial support across all industry departments.

Stefano Giancola serves as the chief technology officer (CTO) at Orchestra Scientific, a company dedicated to innovative solutions for CO2 capture applications. He holds a Ph.D. in Physical Chemistry of Materials from the University of Montpellier (2016). Throughout his career, Dr. Giancola has conducted extensive research in esteemed institutions, including ICIQ (2018–2020), and the universities of Montpellier (2012–2017) and Perugia (2011–2012). His expertise spans various domains, encompassing carbon capture technologies, MOFs, polymers, ionomers, membrane materials, electrospinning, fuel cells, and water electrolyzers. Dr. Giancola has authored numerous publications in high-impact scientific journals, boasting an h-index of 10.

JR Galán-Mascarós received his PhD in Chemistry from University of Valencia (1999). After a postdoctoral stay at Texas A&M University (1999–2001), and a "Ramon y Cajal" fellowship at the Institute of Molecular Science (2002–2008), he moved to the Institute of Chemical Research of Catalonia (ICIQ) in Tarragona, Spain, as ICREA Research Professor, his current position. His research career is essentially multidisciplinary, taking advantage of the tools offered by inorganic chemistry to design novel materials with particular interest in multifunctional smart materials and catalysis for solar fuels. He published over 230 papers and given over 60 invited lectures.